Extreme ultraviolet radiation with coherence time greater than 1 s

Craig Benko[1]*, Thomas K. Allison[1,2], Arman Cingöz[1†], Linqiang Hua[1,3], François Labaye[1], Dylan C. Yost[1†] and Jun Ye[1]*

Many atomic and molecular systems of fundamental interest possess resonance frequencies in the extreme ultraviolet (XUV) where laser technology is limited and radiation sources have traditionally lacked long-term phase coherence. Recent breakthroughs in XUV frequency comb technology have demonstrated spectroscopy with unprecedented resolution at the megahertz level, but even higher resolutions are desired for future applications in precision measurement. By characterizing heterodyne beats between two XUV comb sources, we demonstrate the capability for sub-hertz spectral resolution. This corresponds to coherence times >1 s at photon energies up to 20 eV, more than six orders of magnitude longer than previously reported. This work establishes the ability of creating highly phase-stable radiation in the XUV with performance rivalling that of visible light. Furthermore, by direct sampling of the phase of the XUV light originating from high-harmonic generation, we demonstrate precise measurements of attosecond strong-field physics.

In the infrared, visible and near-ultraviolet spectral regions, the precision and accuracy of frequency metrology[1,2] has vastly exceeded that of traditional spectroscopic methods. Two key enabling laser technologies driving these measurements are ultrastable lasers with long (>1 s) coherence times[3,4] and optical frequency combs[5]. However, for wavelengths below ~200 nm, conventional light sources have short coherence times[6] and are not useful for frequency metrology. Future applications in precision measurement with highly charged ions[7], helium[8], nuclear clocks[9] or hydrogen-like and helium-like ions[10] necessitate phase-stable light in the extreme ultraviolet (XUV). The workhorse of XUV and soft-X-ray science, synchrotron radiation[6], is both temporally and spatially incoherent. New free-electron laser sources have a high degree of spatial coherence, but, due to their single-shot nature, coherence times are never longer than their (femtosecond) pulse durations[11–13]. Conventional XUV lasers[14], based on short-lived population inversions in highly ionized pulsed plasmas, are spatially coherent but also temporally incoherent on scales useful for XUV frequency metrology.

In the last decade, high-order harmonic generation (HHG) using femtosecond lasers has emerged as a method that can support both spatial and temporal coherence in XUV[15], and the use of HHG sources for high-resolution spectroscopy in the XUV has recently been demonstrated at the megahertz level[16–19]. In this Article, we report the observation of coherence times greater than 1 s in the XUV, measured via heterodyne beating between two XUV frequency comb sources based on intracavity HHG[20–22]. Similar to heterodyne interferometry with continuous-wave (c.w.) lasers, our frequency comb lasers in the near-infrared (NIR) are upconverted to the XUV and then combined to form the heterodyne beatnote. The apparatus, shown schematically in Fig. 1a, is analogous to a Mach–Zehnder interferometer, where each arm of the interferometer contains a cavity-enhanced HHG apparatus. The first beamsplitter (the acousto-optic modulator, AOM)

separates the NIR frequency comb, and the second beamsplitter (the beam combiner, Fig. 1d) recombines the XUV frequency combs. The heterodyne signal provides information about the phase of the XUV light and its noise properties. We use the phase information of the heterodyne signal to probe attosecond-timescale, strong-field physics.

XUV comb generation and XUV interferometer

In the experiment, we pumped two independent femtosecond enhancement cavities[20,21,23] (fsECs) with a high-power Yb:fibre frequency comb outputting 120 fs pulses at 154 MHz with an average power of 80 W centred at 1,070 nm (ref. 24). To pump two fsECs the frequency comb was split into two by an AOM so that the two resulting combs had a carrier envelope offset frequency detuning of $\Delta f_{\mathrm{ceo}} = 1$ MHz. Each fsEC (XUV1 and XUV2, Fig. 1a) was actively stabilized using the Pound–Drever–Hall technique with piezo-electric transducers on cavity mirrors as actuators. The carrier envelope offset was not actively stabilized, but its passive stability was sufficient to maintain good power enhancement. Each fsEC typically operated with an average power of ~4.5 kW and a peak intensity of 4×10^{13} W cm^{-2}. Xenon gas for HHG was injected at the cavity foci via quartz nozzles with ~150 μm apertures backed by ~1 atm of pressure. Harmonics were coupled out of the fsECs in a co-linear fashion using 330-μm-thick intracavity sapphire plates set at the Brewster angle for the fundamental radiation to limit intracavity loss. The finesse of the fsECs was intentionally kept low to mitigate the nonlinearities of the Brewster plate and the plasma[22,25,26], but enhancement factors of ~200 were still obtained. The two XUV beams were combined (more on this later) and detected using either an electron multiplier or a photomultiplier tube (PMT) with a phosphor screen. A schematic of the optical layout is shown in Fig. 1a. Because the pump frequency combs were offset by Δf_{ceo}, the resulting XUV frequency comb had a relative detuning of $q \times \Delta f_{\mathrm{ceo}}$ and heterodyne beatnotes could be
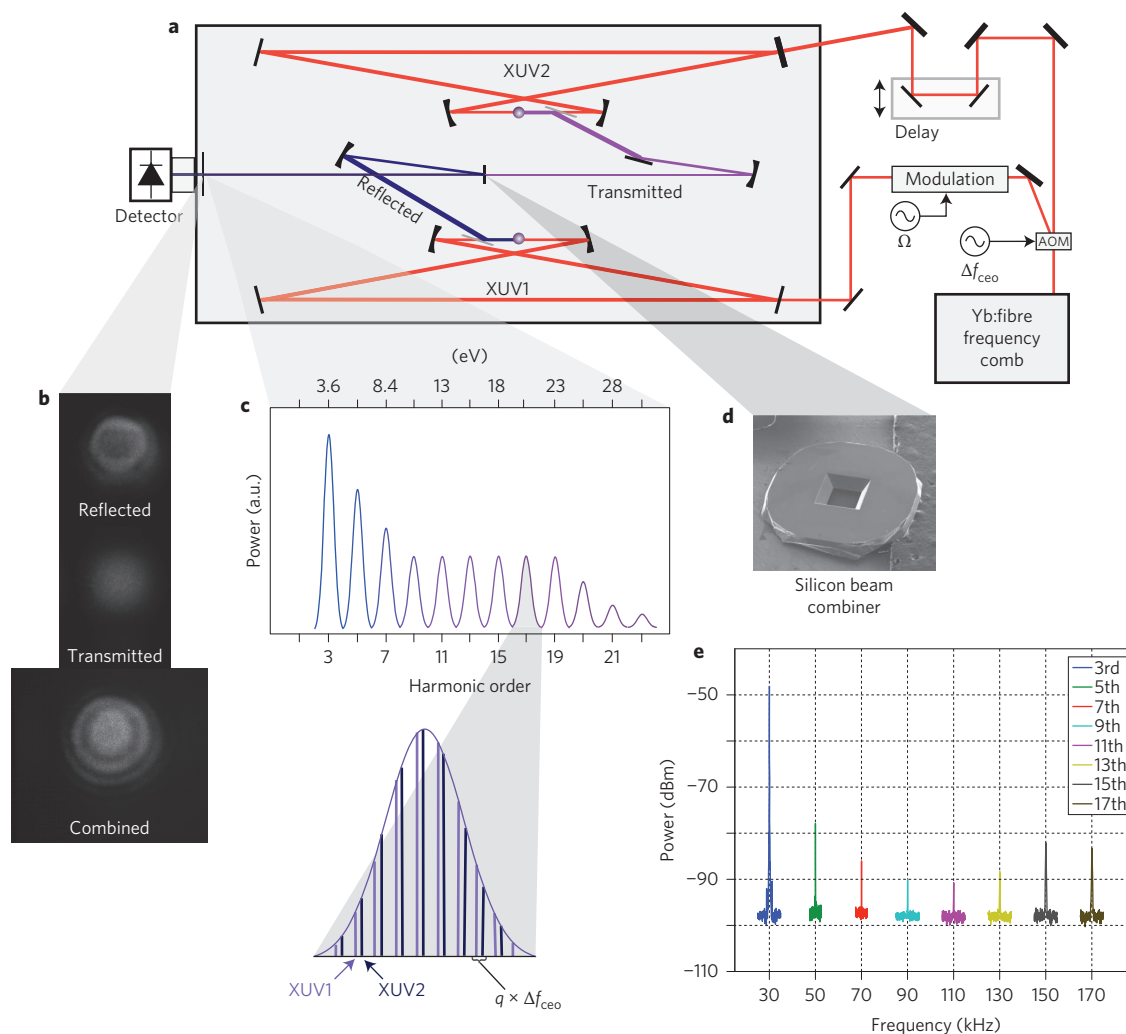
Figure 1 | Schematic of experiment and harmonic spectra. a, A high-powered frequency comb is split with an AOM to create an f_{ceo} shift of 1 MHz. The split beams are then coupled into independent femtosecond enhancement cavities (XUV1, XUV2) to reach intensities suitable for HHG. The harmonic light is coupled out with a Brewster plate and is steered to the beam combiner (shown in **d**) with XUV optics. **b**, Transmitted, reflected and combined beam profiles. The central interference fringe is selected with a spatial filter before detection. **c**, Schematic of the harmonic spectrum. Each harmonic order has a frequency comb structure with teeth spaced by the laser repetition rate. **e**, Measured radiofrequency beatnotes of the 3rd to 17th harmonics. The beatnotes have been mixed down to lower frequencies from $q \times 1$ MHz for clarity. The beatnotes are shown on a 30 Hz resolution bandwidth.

observed at these frequencies, so a series of beatnotes appeared in the radiofrequency output of the detector, effectively mapping the XUV spectrum of the harmonics to the radiofrequency domain (Fig. 1c,e).

Splitting the NIR frequency comb beam at the beginning of the interferometer with the AOM is straightforward, but recombination of the XUV beams at the end of the interferometer is not. Because there are no transparent materials in the XUV, there are no standard beamsplitters available for recombination. Instead, we rely on a wavefront division scheme. A silicon wafer with a $100\ \mu m$ pyramidal aperture produced by KOH etching was used as the beam combiner (Fig. 1d). The beam from XUV2 was focused through the aperture, but the reflected beam from XUV1 is much larger than the aperture. All the optics for the XUV light, including the beam combiner, were coated with boron carbide (B_4C) to enhance their reflectivity in the XUV[27]. In the near field, there was no overlap between the two beams, but in the far field the beams interfered with a circular, 'bulls-eye' fringe pattern (Fig. 1b). The fringe pattern could be easily observed by setting $\Delta f_{ceo} = 0$ and adjusting the relative path length of the interferometer so that pulses from XUV1 and XUV2 overlapped in time at the detector. To observe

beat signals at finite Δf_{ceo}, the central portion of the fringe was selected with an aperture before detection. A key feature of this beam combination scheme is that the fringe period scales weakly as $\sqrt{\lambda}$, so the interferometer can work well over a broad range of wavelengths, allowing us to simultaneously observe beats at the fundamental, the 17th harmonic, and all the harmonics in between.

Because fsECs XUV1 and XUV2 were both pumped by a common NIR laser, the noise in the radiofrequency beatnotes was immune to the common-mode frequency noise of the Yb:fibre laser. Thus, the apparatus directly measured noise from the HHG process or the cavity-plasma dynamics[25]. However, because the interferometer was not actively stabilized, there were small amounts of relative noise induced by vibrations in the optics, giving the two sources a non-zero relative linewidth that is technical in origin.

Phase noise and long coherence time
Here, we show that HHG shares many common features with classical frequency multiplication of radiofrequency signals. In frequency multiplication, the power spectral density (PSD) of the
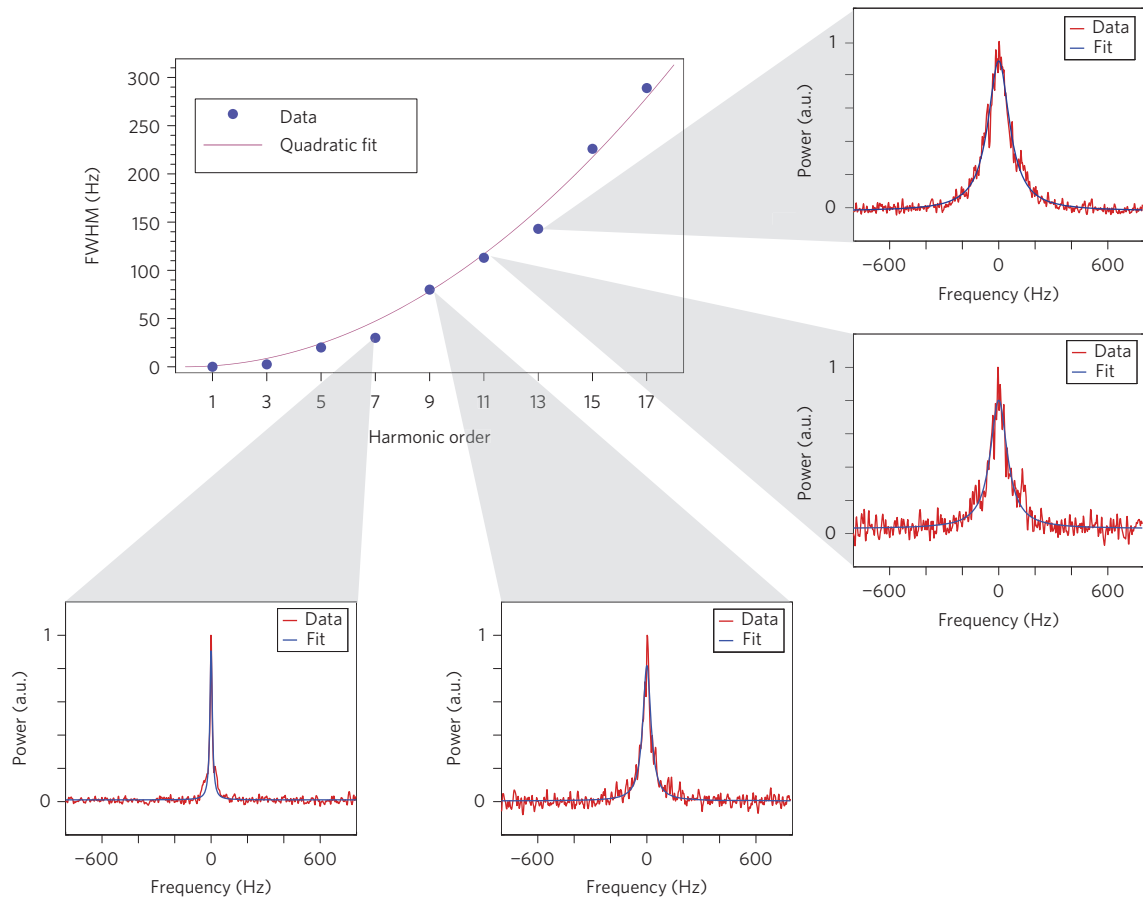
Figure 2 | Linewidth scaling of comb teeth versus harmonic order. The FWHM of the harmonic beatnotes are plotted versus harmonic order. A clear quadratic dependence is shown by the fit.

phase noise $S_\phi(f)$ increases quadratically with harmonic order[28]. Even if the multiplication process is noiseless, any noise around the carrier will still increase with harmonic generation, thus setting a fundamental limit on how phase noise transforms under frequency multiplication and thus the achievable coherence level in the XUV (see Methods). The linewidth of a carrier can be related to $S_\phi(f)$ by the approximation[29]

$$1\,\mathrm{rad}^2 \approx \int_{f_{3\mathrm{dB}}}^{\infty} S_\phi(f)\,\mathrm{d}f \tag{1}$$

The limit of the integral $f_{3\mathrm{dB}}$ is the point where approximately half of the power is in the carrier and half in the noise. Therefore, the 3 dB linewidth of the carrier will increase quadratically with harmonic order. If one is not careful to have a low-noise carrier before multiplication, the carrier will start to disappear, leading to the known phenomenon of carrier collapse[30]. Figure 2 shows the full-width at half-maximum (FWHM) of each harmonic comb tooth plotted versus harmonic order. A simple fit to FWHM = aq^2, where a is the scaling parameter, highlights the quadratic dependence of the linewidth. The linewidth dependence on harmonic order was also independent of intracavity power. This analysis shows that there is a fundamental scaling of phase noise from the generating laser to the resulting XUV light. For example, assuming the best available c.w. laser with a linewidth of 30 mHz (ref. 4) and that the fundamental comb will faithfully follow the phase of the c.w. laser[31], the linewidth at the 17th harmonic would be 8.7 Hz. Fortunately for HHG, we do not observe any additional linewidth-broadening mechanisms other than the unavoidable classical frequency multiplication scaling.

We show that the previously observed linewidth originated from the differential path noise and not HHG physics, so higher levels of coherence can be observed. The differential path length noise in the interferometer can be removed by phase-stabilizing the two optical paths. A small amount of pump light leaks through the XUV optics to the detection plane, which is then picked off and detected on a photodetector to provide an error signal sensitive to interferometer fluctuations. The error signal is filtered and used to apply feedback correction to the AOM frequency, thus removing the relative noise (see Methods). With the interferometer phase locked, we can probe any noise processes intrinsic to intracavity HHG. A dramatic change in the linewidth of the XUV beatnotes is observed with a stable interferometer. The unstabilized beatnote of the pump laser and the beatnote at the 17th harmonic are shown in Fig. 3a,c and the corresponding stabilized case in Fig. 3b,d with a 250 mHz resolution bandwidth. Similar resolution limited beats were observed on the 3rd − 19th harmonic. The coherence of the pump lasers is faithfully transferred to the harmonics as seen by the resolution-limited beatnote of 62.5 mHz in Fig. 3f. This is equivalent to a coherence time of 16 s or a stable phase relation maintained over ∼1 × 10^9 consecutive pulses. This is a nearly seven orders of magnitude larger coherence time than ever reported in the XUV[16,18,32]. This establishes that our XUV comb system is extremely phase-coherent and has the capability to support sub-hertz coherences in the XUV. Furthermore, by also observing coherent beats from harmonics generated from xenon gas in one cavity and krypton in the other (Fig. 3e), we demonstrate that the common-mode noise rejection of this measurement scheme is not conditioned on the two XUV comb systems being identical.
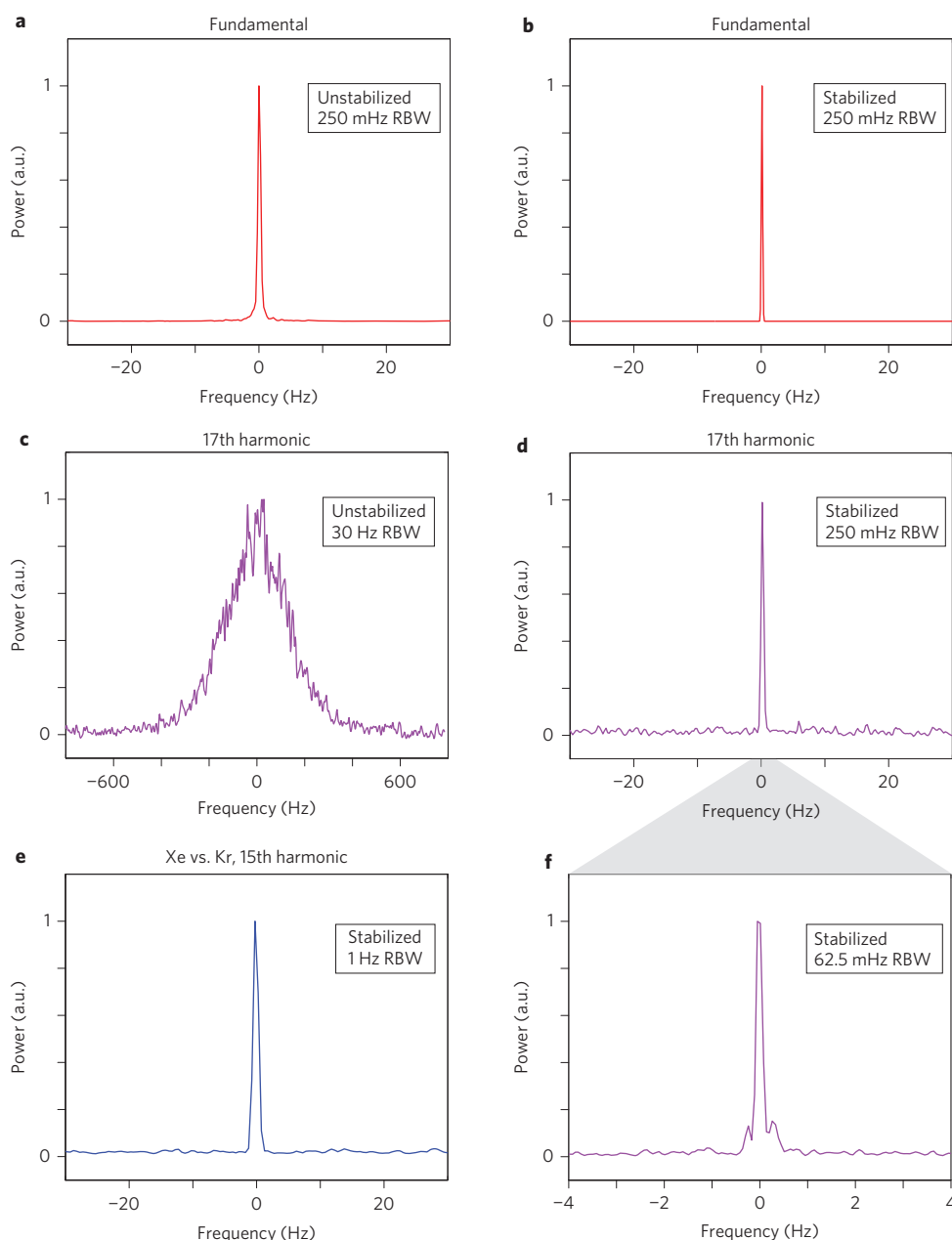
Figure 3 | Demonstration of sub-hertz coherence in the XUV. a,c, Unstabilized beatnotes of the pump laser and the 17th harmonic. **b,d,** Stabilized beatnotes of the pump laser and the 17th harmonic. **e,** Comparison of the two sources when one is injected with krypton and the other with xenon. A 1 Hz resolution bandwidth limited signal is achieved. **f,** The resolution of the 17th harmonic can be improved further to a 62.5 mHz resolution bandwidth showing a coherence time of >16 s. RBW, resolution bandwidth.

Application to attosecond strong-field physics

The heterodyne beatnotes in the XUV provide unique and unprecedented access to the phase of XUV radiation. We can use this to probe attosecond physics and measure the intensity-dependent dipole phase[33]. This technique is a fundamentally different method for probing this phenomenon than used in previous realizations and does not rely on extensive spatial and spectral filtering to observe interference between multiple quantum pathways[32,34]. Furthermore, this technique does not rely on referencing the short to long trajectory contributions, or vice versa[35]. It is complementary to RABBITT and related methods based on photoelectron spectroscopy[36–38], which seek to determine the time delay (or equivalently phase shift) between adjacent harmonic orders at a given intensity. In this experiment, we isolate individual harmonics and precisely measure their phase shift as a function of intensity.

These phase shifts can be directly linked to the temporal dynamics of the electron in the intense laser field[36]. By using amplitude modulation (AM) on one arm of the interferometer, we can measure the amount of induced phase modulation (PM) on the XUV light (see Methods). For this measurement, the peak intensity of the modulated cavity was 3.4×10^{13} W cm^{-2}, with a 15% AM depth. The intensity-dependent dipole phase can be expressed as

$$\phi = -\alpha_j \frac{U_p(I)}{\omega} = -\alpha_j \frac{I}{4\omega^3} \quad (2)$$

where I is the laser intensity, $U_p(I)$ the pondermotive energy, ω the laser frequency, ϕ the phase of the emitted XUV light and α_j is the phase coefficient. As a result of our on-axis spatial filtering (needed to observe a high-contrast beatnote) we are primarily sensitive to the
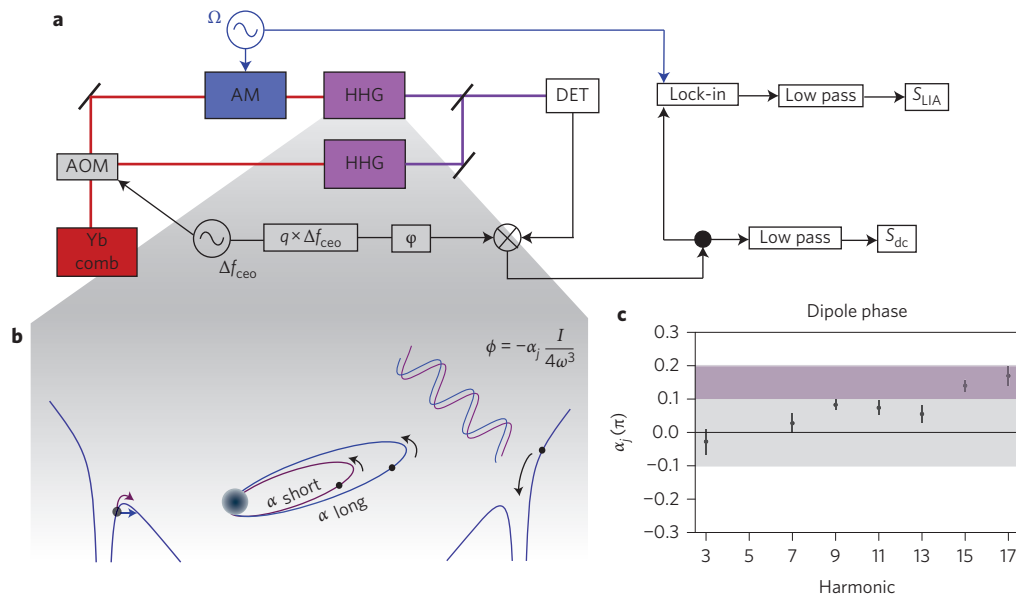
Figure 4 | Measurement of intensity-dependent dipole phase. a, Schematic of signal pathway. A two-step demodulation process is necessary to detect the PM on the XUV light induced by AM on the pump laser. **b**, After an electron is ionized, it accelerates in the electric field. Two dominant quantum trajectories (short and long) are important for the XUV emission, where the phase of the light depends directly on the intensity of the electric field and its quantum path. **c**, Intensity-dependent phase of the atomic dipole for the short trajectory of the 3rd to 17th harmonics. The grey area is the predicted region where the below-threshold harmonic intensity-dependent phase can fall. The purple shaded region is where the above-threshold intensity-dependent phase is predicted to lie.

short trajectory. The schematic of the measurement is shown in Fig. 4a. The measurement requires a two-step demodulation process to extract the amount of PM induced on the XUV light from the AM applied to the pump laser. Great care was taken to ensure that the amount of PM on the XUV light was not induced by parasitic PM on the pump laser (see Methods). The phase of the XUV light depends on both the intensity of the light and the particular quantum path the electron traverses (Fig. 4b). The result of the measurement is shown in Fig. 4c, where the α_j of equation (2) is expressed in atomic units according to the convention of Yost and co-authors[32]. The shaded purple region corresponds to values predicted by the standard semi-classical model (SCM)[33]. The grey shaded region represents the range of values predicted by different approximations to below-threshold harmonics[39].

Below threshold, short-trajectory harmonics do not originate from tunnel ionization as in the above-threshold case and are much more sensitive to the atomic potential and ionization dynamics[39]. Our measurement is able to discriminate between contributions of the standard SCM[33] and a model that includes over-the-barrier (OTB) ionization[39] to confirm that the below-threshold harmonics mostly originate from OTB ionization. Furthermore, our measurement for an above-threshold harmonic (15th and 17th) agrees well with the predictions of the SCM[33] and the below-threshold with the predictions of Yost and co-authors[32] and the theoretical framework of Hostetter and co-authors[39]. Further exploration of intensity-dependent phases in atoms and molecules with comparison to calculations is the subject of future work. Our phase measurement technique was able to resolve phase shifts with uncertainties at the 10^{-2} rad level, which corresponds to a time uncertainty of ~6 as. In contrast to typical experiments that utilize direct attosecond timing resolution[38], we measure the attosecond electron dynamics imprinted on the phase of the emitted XUV light originating from HHG[36]. With system improvements, it is feasible to extend this into the ≤ 1 as regime, rivalling the highest achievable temporal resolution of attosecond electron dynamics[36,40]. Thus, our apparatus provides direct, unambiguous access to the phase of XUV radiation

and will prove to be a valuable tool for attosecond science and the dynamics of atoms and molecules in intense laser fields.

Summary and future outlook

We have demonstrated that HHG is extremely phase-coherent. We have identified the primary noise requirements on the pump laser and shown that it is possible to support coherence times greater than 1 s in the XUV. We have also developed an interferometer capable of operating from 1,070 nm to 56 nm, but with different optics and a new beam combiner[41], extension to even shorter wavelengths is possible. Such an apparatus will be a vital tool for future work in dual-comb spectroscopy, Fourier transform spectroscopy[42], high-resolution molecular spectroscopy[43], attosecond electron dynamics in intense laser fields[44] and HHG spectroscopy[45]. We have successfully probed physics at attosecond timescales using the tools of frequency metrology to measure the intensity-dependent dipole phase. Future work will require improved output coupling[46–48] and power-scaling[17,49,50] schemes to extend the high level of phase coherence to shorter wavelengths, possibly enabling spectroscopy of a nuclear isomer transition where highly phase-stable light will be needed for excitation.

Methods

AOM and beat detection. To create a small frequency offset between the two XUV sources we relied on an AOM to frequency-shift the pump laser such that the relative detuning was 1 MHz. Because there are no available AOMs at this frequency, we drove the AOM such that 1 MHz $= f_{rep} - f_{AOM}$. Two beats at frequencies less than f_{rep}, one at f_{AOM} and the conjugate at $f_{beat} = f_{rep} - f_{AOM}$ were therefore observed. The conjugate beatnote is sensitive to any noise in f_{rep}. To remove this, we derived f_{AOM} by phase-locking a voltage-controlled oscillator to f_{rep} detuned by 1 MHz such that $f_{AOM} = f_{rep} - 1$ MHz. This removed the dependence of f_{rep} from the conjugate beatnote and put it in f_{AOM}. Accordingly, the low-frequency beatnote can be detected noise-free where we have detectors of adequate bandwidth.

Phase noise. A signal oscillating at frequency ω with PM can be expressed as

$$A = A_0 e^{-i\omega t - i\beta \sin(\omega_m t)} \qquad (3)$$

where β is the modulation depth and ω_m is the modulation frequency. When β is small, we can express the power in the first-order modulation sideband (SB) relative

to the carrier (C) by $P_{SB}/P_C = (J_1(\beta)/J_0(\beta))^2 \approx J_1(\beta)^2$, where J_n are Bessel functions. We can extend this to the case of general PM and not at a particular discrete tone by $P_{SB}/P_C \approx (1/2)\Delta\phi_{rms}^2$. We can define the phase noise power spectral density as the noise around a carrier within a bandwidth (BW) as

$$S_\phi(f)\left[\frac{rad^2}{Hz}\right] \equiv \frac{1}{2}\frac{\Delta\phi_{rms}^2(f)}{BW} \tag{4}$$

By integrating $S_\phi(f)$, one arrives at equation (1) and gets the approximate linewidth of a signal. The f_{3dB} point is the cutoff of the integral where there is approximately half the power in the carrier and half in the noise.

Phase-stable interferometer. The XUV light is very sensitive to path length fluctuations and any phase fluctuations in the driving laser. It is therefore imperative to keep the interferometer stable to generate the highest levels of coherence in the XUV. The passive stability is sufficient for sub-kilohertz levels of coherence. To stabilize the interferometer, we used the small amount of pump laser light that co-propagates with the XUV light. Because the pump light diverges more than the XUV light, it was simple to separate it out before the detection plane. A small amount of light was picked off and sent to a photodetector where a 1 MHz beatnote was used to measure the phase fluctuations in the interferometer caused by mechanical noise on the mirrors. The beatnote was mixed with a radiofrequency synthesizer to generate an error signal. The error signal was filtered and the correction signal was applied to the 1 MHz reference frequency for the AOM. Because the fluctuations of the interferometer were small, the phase-lock loop that sets the AOM frequency could easily compensate for the small, necessary corrections.

Measurement of intensity-dependent dipole phase. The intensity-dependent dipole phase is expressed in equation (2). By trying to measure the intensity-dependent phase that results from HHG, we are effectively measuring the AM–PM coupling, with the AM being on the pump laser and the PM being on the XUV light. We can mathematically describe a beatnote signal as

$$S(t) = [1 + A\sin(\Omega t + \phi_m)]\cos(\omega t + P\sin(\Omega t + \phi_m)) \tag{5}$$

where ω is the frequency of the beatnote, Ω is the frequency of the applied modulation and ϕ_m is its phase, A is the AM depth and P is the PM depth. Each beatnote is characterized by its own values for A and P. To avoid confusion, the subscripts will refer to which signal it represents. For example, A_{IR} is for the AM of the pump laser and P_q is the PM of the qth harmonic. Our task is to determine the values for A and P at the pump and the harmonics. By taking the ratio of P_q to A_{IR} and using proper units, we can extract the intensity-dependent phase coefficient α_j.

We need to simultaneously extract the relevant parameters of equation (5) at both the harmonic of interest and the IR. To do this, we use a two-step demodulation process. By taking equation (5) and mixing it with a stable radiofrequency signal (LO1) at a frequency of ω and relative phase offset ϕ, we obtain

$$S(t) \otimes V_1\cos(\omega t + \phi) = S_1(t) \tag{6}$$

$$S_1(t) \approx V_1\left(\cos(\phi) - \frac{AP}{2}\sin(\phi) + A\cos(\phi)\sin(\Omega t + \phi_m) - P\sin(\phi)\sin(\Omega t + \phi_m)\right) \tag{7}$$

We have ignored terms at 2ω. We can further low pass the signals at Ω and obtain a 'd.c.' signal

$$S_1(t) \xrightarrow{\text{Low pass}} S_{dc} = V_1\left(\cos(\phi) - \frac{AP}{2}\sin(\phi)\right) \tag{8}$$

Equation (8) will be one of our primary signals. Note that the phase is set by the phase of LO1. This also assumes that the phase of the XUV beatnote is stable. This is true when we phase-stabilize our interferometer.

The signal $S_1(t)$ contains terms that oscillate at the applied modulation frequency Ω. We can demodulate our signal once more using a lock-in amplifier at the correct phase ϕ_m and ignore terms at 2Ω to obtain

$$S_1(t) \otimes V_2\sin(\Omega t + \phi_m) = S_{LIA} \approx V_1 V_2(A\cos(\phi) - P\sin(\phi)) \tag{9}$$

where S_{LIA} is our second signal. With equation (8), equation (9) and some independently measured parameters (for example, the existing AM–AM coupling), we can extract our parameters of interest. To measure the A_{IR}–A_q coupling, we can use our beatnote signals. Our XUV beatnotes are directly proportional to the amount of XUV power in each beam. The amount of beatnote power can also be easily measured on a radiofrequency spectrum analyser. By changing the amount of power in one of the enhancement cavities and observing how the beatnote power changes, we can determine how much the XUV power must have changed for a

given laser intensity change. A_q can be determined by

$$\Delta dB = 20\log_{10}(1/\sqrt{x}) \tag{10}$$

$$A_q = 1 - x \tag{11}$$

where ΔdB is the measured beatnote power. By applying AM to the pump laser on one arm of the interferometer, we can control A_{IR} very well. It is also easily measured with a photodetector. By varying the phase of LO1, we can measure S_{dc} and S_{LIA} (equations (8) and (9)) simultaneously. With the modulation (A,P) turned off, S_{dc} tells us the phase of the beat. With the modulation on, the relative phase between S_{dc} and S_{LIA} can tell us the ratio A/P. Because A can be measured independently, we can extract the amount of PM, P. This procedure needs to be done with the infrared signal and the XUV signal simultaneously to prevent any systematic errors.

The results of the measurements are shown in Fig. 4c. Each data point is the average of approximately ten runs of data where equations (8) and (9) were measured while varying the phase ϕ of LO1 from 0 to 2π. The measured values for P_q were corrected for any parasitic P_{IR} using $P_q \to P_q - q \times P_{IR}$.

Signal correction. The signal correction of $P_q \to P_q - q \times P_{IR}$ is justified by experimental observations. First, the quadratic scaling of the linewidth shows that the phase of the XUV light is directly linked to the phase of the NIR light. Any phase shift $\Delta\phi$ in the NIR is $q \times \Delta\phi$ at the qth harmonic. For the beatnote signals, this also implies that the PM depth P_q is related to the modulation depth in the NIR by $P_q = q \times P_{IR}$. This relation is also justified by observing the beatnote signals in the presence of PM on the NIR laser. By measuring the amount of PM on the NIR laser and the amount induced on the XUV beatnotes via the relation of the carrier to the modulation sideband heights, we have verified the relation $P_q = q \times P_{IR}$. Our lock-in detection methods also produce the same relation when additional PM is placed on the NIR laser.

Modulation effects. Modulating the intensity has notable effects on the neutral/plasma density ratio inside the enhancement cavity. However, the modulation is slow at 2 kHz and the cavity feedback loop can easily follow it to maintain resonance. The effect has been systematically studied previously[25]. Due to the neutral/plasma density changes, there is a small amount of PM induced by AM on the NIR laser. This was verified by measuring the effect with gas present and absent. This can easily corrupt the intensity-dependent phase measurement and necessitates the correction described previously. Furthermore, any cavity oscillation due to bistability[25] can render the signals too noisy. Therefore, by careful measurement of the PM on the NIR laser and the XUV beatnotes, we can extract the intensity-dependent phase originating from HHG and not other macroscopic effects.

References

1. Udem, Th. *et al.* Optical frequency metrology. *Nature* **416,** 233–237 (2002).
2. Bloom, B. J. *et al.* An optical lattice clock with accuracy and stability at the 10^{-18} level. *Nature* **506,** 71–75 (2014).
3. Kessler, T. *et al.* A sub-40-mHz-linewidth laser based on a Silicon single-crystal optical cavity. *Nature Photon.* **6,** 687–692 (2012).
4. Bishof, M. *et al.* Optical spectrum analyzer at the atomic quantum projection noise limit. *Phys. Rev. Lett.* **111,** 093604 (2013).
5. Cundiff, S. & Ye, J. Femtosecond optical frequency combs. *Rev. Mod. Phys.* **75,** 325–342 (2003).
6. Attwood, D. T. *Soft X-rays and Extreme Ultraviolet Radiation* (Cambridge Univ. Press, 2007).
7. Berengut, J. C. *et al.* Electron–hole transitions in multiply charged ions for precision laser spectroscopy and searching for variations in α. *Phys. Rev. Lett.* **106,** 210802 (2011).
8. Eyler, E. E. *et al.* Prospects for precision measurements of atomic helium using direct frequency comb spectroscopy. *Eur. Phys. J. D* **48,** 43–55 (2007).
9. Campbell, C. J. *et al.* Single-ion nuclear clock for metrology at the 19th decimal place. *Phys. Rev. Lett.* **108,** 120802 (2012).
10. Herrmann, M. *et al.* Feasibility of coherent XUV spectroscopy on the ^{1}S–^{2}S transition in singly ionized helium. *Phys. Rev. A* **79,** 052505 (2009).
11. Ackermann, W. *et al.* Operation of a free-electron laser from the extreme ultraviolet to the water window. *Nature Photon.* **1,** 336–342 (2007).
12. Young, L. *et al.* Femtosecond electronic response of atoms to ultra-intense X-rays. *Nature* **466,** 56–61 (2010).
13. Emma, P. *et al.* First lasing and operation of an Ångstrom-wavelength free-electron laser. *Nature Photon.* **4,** 641–647 (2010).
14. Suckewer, S. & Skinner, C. Soft X-ray lasers and their applications. *Science* **247,** 1553–1557 (1990).
15. Bellini, M. *et al.* Temporal coherence of ultrashort high-order harmonic pulses. *Phys. Rev. Lett.* **81,** 297–300 (1989).

16. Cingöz, A. *et al.* Direct frequency comb spectroscopy in the extreme ultraviolet. *Nature* **482,** 68–71 (2012).
17. Yost, D. C. *et al.* Power optimization of XUV frequency combs for spectroscopy applications. *Opt. Express* **19,** 23483–23493 (2011).
18. Kandula, D. Z. *et al.* Extreme ultraviolet frequency comb metrology. *Phys. Rev. Lett.* **105,** 063001 (2010).
19. Morgenweg, J. *et al.* Ramsey-comb spectroscopy with intense ultrashort laser pulses. *Nature Phys.* **10,** 30–33 (2013).
20. Jones, R. J. *et al.* Phase-coherent frequency combs in the vacuum ultraviolet via high-harmonic generation inside a femtosecond enhancement cavity. *Phys. Rev. Lett.* **94,** 193201 (2005).
21. Gohle, C. *et al.* A frequency comb in the extreme ultraviolet. *Nature* **436,** 234–237 (2005).
22. Mills, A. *et al.* XUV frequency combs via femtosecond enhancement cavities. *J. Phys. B.* **45,** 142001 (2012).
23. Jones, R. J. & Ye, J. Femtosecond pulse amplification by coherent addition in a passive optical cavity. *Opt. Lett.* **27,** 1848–1850 (2002).
24. Ruehl, A. *et al.* 80 W, 120 fs Yb-fiber frequency comb. *Opt. Lett.* **35,** 3015–3017 (2010).
25. Allison, T. K. *et al.* Extreme nonlinear optics in a femtosecond enhancement cavity. *Phys. Rev. Lett.* **107,** 193903 (2011).
26. Carlson, D. R. *et al.* Intracavity ionization and pulse formation in femtosecond enhancement cavities. *Opt. Lett.* **36,** 2991–2993 (2011).
27. Vidal-Dasilva, M. *et al.* Electron-beam deposited boron coatings for the extreme ultraviolet. *Appl. Opt.* **47,** 2926–2930 (2008).
28. Walls, F. L. & Demarchi, A. RF spectrum of a signal after frequency multiplication; measurement and comparison with a simple calculation. *IEEE Trans. Instrum. Meas.* **24,** 210–217 (1975).
29. Hall, J. L. in *Proceedings of the International School of Physics—Enrico Fermi* (eds Arimondo, E., Phillips, W. D. & Strumia, F.) 671–702 (North-Holland, 1992).
30. Telle, H. R. in *Frequency Control of Semiconductor Lasers* (eds. Ohtsu, M.) 137–167 (Wiley, 1996).
31. Schibli, T. R. *et al.* Optical frequency comb with sub-millihertz linewidth and more than 10 W average power. *Nature Photon.* **2,** 355–359 (2008).
32. Yost, D. C. *et al.* Vacuum-ultraviolet frequency combs from below-threshold harmonics. *Nature Phys.* **5,** 815–820 (2009).
33. Lewenstein, M. *et al.* Phase of the atomic polarization in high-order harmonic generation. *Phys. Rev. A* **52,** 4747–4754 (1995).
34. Zaïr, A. *et al.* Quantum path interferences in high-order harmonic generation. *Phys. Rev. Lett.* **100,** 143902 (2008).
35. Corsi, C. *et al.* Direct interferometric measurement of the atomic dipole phase in high-order harmonic generation. *Phys. Rev. Lett.* **97,** 023901 (2006).
36. Mairesse, Y. *et al.* Attosecond synchronization of high-harmonic soft X-rays. *Science* **302,** 1540–1543 (2003).
37. Sansone, G. *et al.* Measurement of harmonic phase differences by interference of attosecond light pulses. *Phys. Rev. Lett.* **94,** 193903 (2005).
38. Chang, Z. *Fundamentals of Attosecond Optics* 1st edn (CRC Press, 2011).
39. Hostetter, J. *et al.* Semiclassical approaches to below-threshold harmonics. *Phys. Rev. A* **82,** 23401 (2010).
40. Krausz, F. & Ivanov, M. Attosecond physics. *Rev. Mod. Phys.* **81,** 163–234 (2009).
41. Agåker, M. *et al.* Novel instruments for ultra-soft X-ray emission spectroscopy. *Nucl. Instrum. Meth. A* **601,** 213–219 (2009).
42. Keilmann, F. *et al.* Time-domain mid-infrared frequency-comb spectrometer. *Opt. Lett.* **29,** 1542–1544 (2004).
43. Hinnen, P. *et al.* XUV-laser spectroscopy of HD at 92–98 nm. *Phys. Rev. A* **52,** 4425–4433 (1995).
44. Shafir, D. *et al.* Resolving the time when an electron exits a tunneling barrier. *Nature* **485,** 343–346 (2013).
45. Itatani, J. *et al.* Tomographic imaging of molecular orbitals. *Nature* **432,** 867–871 (2004).
46. Moll, K. D. *et al.* Output coupling methods for cavity-based high-harmonic generation. *Opt. Express* **14,** 8189–8197 (2006).
47. Pupeza, I. *et al.* Compact high-repetition-rate source of coherent 100 eV radiation. *Nature Photon.* **7,** 608–612 (2013).
48. Yost, D. C. *et al.* Efficient output coupling of intracavity high-harmonic generation. *Opt. Lett.* **33,** 1099–1101 (2008).
49. Lee, J. *et al.* Optimizing intracavity high harmonic generation for XUV fs frequency combs. *Opt. Express* **19,** 23315–23326 (2011).
50. Carstens, H. *et al.* Megawatt-scale average-power ultrashort pulses in an enhancement cavity. *Opt. Lett.* **39,** 2595–2598 (2014).

Author contributions

C.B., T.K.A., A.C., D.C.Y. and J.Y. contributed to the design and planning of the experiment. C.B., L.H. and F.L. acquired the data. C.B., T.K.A., L.H., F.L. and J.Y. analysed the data. All authors discussed the results and contributed to the writing of the final manuscript.

Additional information

Reprints and permissions information is available online at www.nature.com/reprints. Correspondence and requests for materials should be addressed to C.B. and J.Y.

Competing financial interests

The authors declare no competing financial interests.